



Contents lists available at [ScienceDirect](https://www.sciencedirect.com)

Journal of Biomechanics

journal homepage: [www.elsevier.com/locate/jbiomech](http://www.elsevier.com/locate/jbiomech)



## Simulation of multi-curve active catheterization for endovascular navigation to complex targets

Arif Badrou<sup>a</sup>, Nicolas Tardif<sup>a</sup>, Philippe Chaudet<sup>a</sup>, Nathan Lescanne<sup>b</sup>, Jérôme Szewczyk<sup>b,c</sup>, Raphaël Blanc<sup>b,d</sup>, Nahiène Hamila<sup>e</sup>, Anthony Gravouil<sup>a</sup>, Aline Bel-Brunon<sup>a,\*</sup>

<sup>a</sup> Univ Lyon, INSA Lyon, CNRS, LaMCoS, UMR5259, 69621 Villeurbanne, France

<sup>b</sup> BaseCamp Vascular (BCV), 75005 Paris, France

<sup>c</sup> Sorbonne Université, CNRS, INSERM, Institut des Systèmes Intelligents et de Robotique, ISIR, ISIR - AGATHE, F-75005 Paris, France

<sup>d</sup> Department of Interventional Neuroradiology, Fondation Rothschild Hospital, Paris, France

<sup>e</sup> Ecole Nationale d'Ingénieurs de Brest, ENIB, UMR CNRS 6027, IRDL, F-29200, Brest, France

### ARTICLE INFO

#### Keywords:

Aorta  
Endovascular navigation  
Shape Memory Alloy  
Catheter  
Modeling

### ABSTRACT

The recent development of endovascular therapies has been accompanied by increasingly accurate navigation simulations to assist surgeons in decision making processes or to produce training tools. However, they have been focused mostly on targets within the aortic vasculature. In order to reach complex targets such as cerebral arteries by endovascular navigation, an active guidewire made of a Shape Memory Alloy (SMA) was recently proposed. The active part becomes deformed by the Joule effect and this deformation induces a bending of the guidewire. This setup is particularly suited for facilitating the access to Supra-Aortic Trunks (SATs) and, in our case, especially the left carotid artery. A complete characterization of the endovascular active navigation was conducted. In this framework, a test bench was developed to obtain an order of magnitude of the velocities applied on the guidewire as well as on the passive catheter going along with it in endovascular navigation. A numerical model was developed and validated in the case of navigation in a complex phantom aorta. We succeeded in representing crucial phenomena observed experimentally: snapping, active curvatures, interactions between the tools. In the last part of this study, it was demonstrated that adapting the guidewire design made it possible to hook the left carotid on three complex aortas.

### 1. Introduction

There has been a development of endovascular treatments in recent years. The introduction of minimally invasive surgery has led to reduce mortality and morbidity rates compared with open procedures (Verhage et al., 2009). The development of such techniques has been accompanied by more and more numerical simulations for decision support (Gindre et al., 2016; Perrin et al., 2014; Auricchio et al., 2013) or as training tools (Westwood, 2005; Nesbitt et al., 2016; Alderliesten et al., 2004; See et al., 2016). Among them, few are related to the navigation of tools, i.e., guidewires and catheters, in the aorta to reach the target to treat. In Mouktadiri et al. (2013); Gindre et al. (2016); Mohammadi et al. (2018); Kaladji et al. (2013); Roy et al. (2014) models were developed to predict arterial deformations during surgical tools navigation in the framework of aortic aneurysm. In Menut (2017) the simulation of navigation tools was adapted to the thoracic aorta. Vy et al. (2018) developed a patient-specific model to predict guidewire deformation on the first stage of a transcatheter aortic valve implantation.

These works involve passive tools where their curvature only depends on their interactions with the aortic wall. The use of such passive devices is adequate in most cases, but in 20% of endovascular therapies, the areas to treat are so-called *complex* due to large tortuosities, e.g., at the Supra-Aortic Trunks (SATs) level, and the navigation may fail (Madhwal et al., 2008; Macdonald et al., 2009; Lam et al., 2007).

Recently, in order to reach complex targets, active devices have been developed. These steerable devices can be made of Shape Memory Alloys (SMAs) (Wayman and Duerig, 1990; Ali et al., 2020; Haga et al., 1998), but other magnetic or electrostrictive materials are also used to curve the guidewires (Ganet et al., 2015; Hwang et al., 2020).

An active guidewire composed of a SMA was designed to facilitate the access to complex areas including SAT in an interventional neuroradiology context (Couture and Szewczyk, 2017; Szewczyk et al., 2011; Szewczyk, 2011). It was made of a long steel shaft and a blade-shaped distal tip on which a Nitinol wire was attached. The combination of wire and blade is called an active part. By applying

\* Corresponding author.

E-mail address: [aline.bel-brunon@insa-lyon.fr](mailto:aline.bel-brunon@insa-lyon.fr) (A. Bel-Brunon).

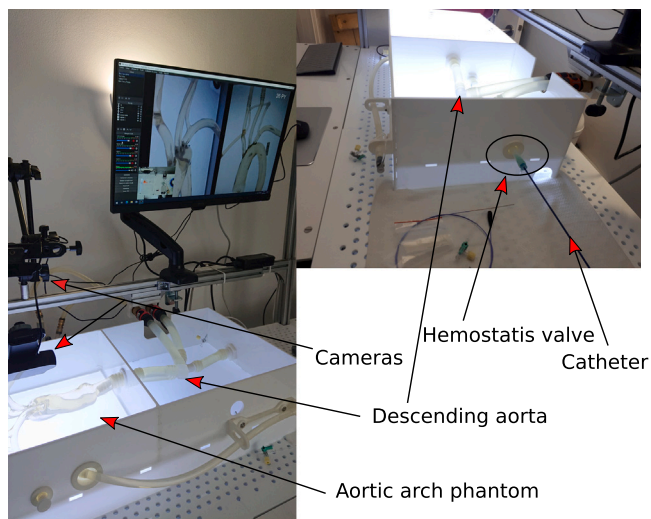


Fig. 1. Overview of the phantom aorta test bench used at BCV.

an electric current, the wire heats up by the Joule effect. The Shape Memory Effect (SME) inherent to SMAs thus causes the wire to shrink (Lagoudas, 2008; Maynadier et al., 2011) forcing the distal tip to bend. This controlled curvature facilitates the navigation through tortuous endovascular paths.

The insertion of the guidewire is followed by the insertion of a Distal Access Catheter (DAC) (Spiotta et al., 2011) that generally exhibits a rigidity gradient along its length to ease its navigation (Gindre et al., 2016; Mouktadiri et al., 2013). The success of navigation is driven by the mechanical behavior of the inserted tools and their co-manipulation.

The aim of the present study was to develop a numerical simulation of the navigation of the active guidewire and DAC towards complex targets. Our success criterion is the ability to *catheterize* the left carotid. The model was confronted with phantom experiments on three complex patient-specific cases. Based on existing studies on endovascular navigation, the main contributions of this work concerned: (i) active navigation to complex targets leading to original navigation scenarios, including the simulation of snapping, and (ii) measurements of clinical gestures thanks to an original bench test. Herein, we first detail the navigation features observed and measured on a dedicated set up. Then, the numerical model of this navigation is described. Finally, results are presented and discussed.

## 2. Characterization of the endovascular navigation on phantom aorta

Navigation towards complex targets is an elaborated combination of gestures and co-manipulations of tools. To get a better insight in this procedure and build the navigation model, this section presents observations and measurements of navigation features performed on a test bench.

### 2.1. The test bench

We aimed at simulating the navigation of the devices in the same conditions as those on the test bench at the French company BaseCamp Vascular (BCV) that developed the active guidewire. The test bench consisted of a module with two boxes: one containing the aortic arch, the other comprising a cylinder representing the descending aorta (see Fig. 1). Any phantom of aortic arch can be mounted in the first box.

The vascular structure was immersed in a mixture of washing liquid and water. A flow of 250L/h was imposed inside the aorta to represent

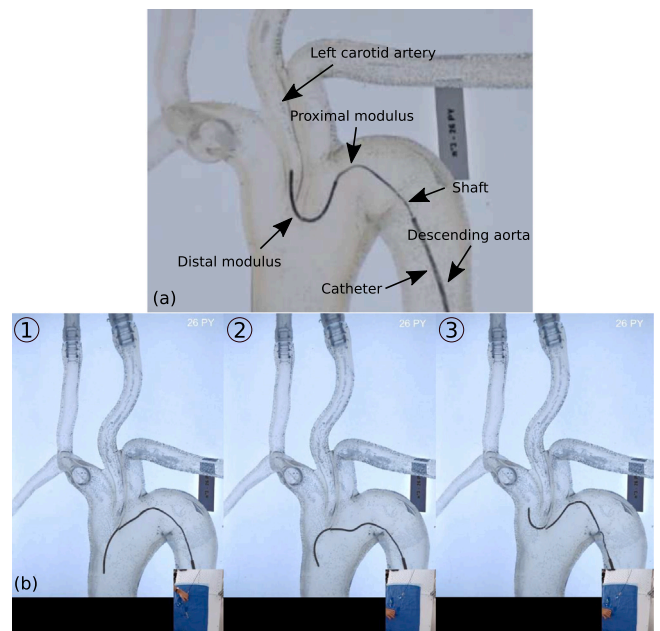


Fig. 2. Focus on the activation of the guidewire and illustration of the snapping effect: (a) activation of a so-called double-deck guidewire: two active parts are visible in the figure, the wires of the active parts are arranged on both sides of the blade so that the double activation tends to snake the guide, (b) illustration of the snapping effect: (1) The guidewire is in contact with the aorta distally (2) Both moduli are activated and a rotation is imposed on the shaft (3) The snapping occurs and the distal part of the guidewire points to the opposite side.

the blood stream, which is rather low and constant compared to the pulsed flow occurring in reality (Hashimoto and Ito, 2010; Sochi, 2013).

### 2.2. Active navigation and snapping effect

The navigation goal was to enter the aortic arch through the descending aorta (assuming femoral access) and to hook the left carotid artery which leads to the brain. The aforementioned active guidewire was used with the combination of the Navien A+ intracranial catheter and the introducer Neuron MAX. Fig. 2 displays the guidewire with two activated moduli showing the S-curvature used to facilitate the navigation through aortas.

Active navigation involves different movements including:

1. Pushing, pulling and rotating the guidewire;
2. Activating the distal active flexions;
3. Pushing the DAC to reach the target area.

During navigation, clinicians often use a buckling phenomenon called *snapping*, which can be described as follows: when the distal part of the guidewire is in contact with the aorta, the activation of both the distal and the proximal active parts, accompanied by a rotation gesture operated by the handler, leads to a sudden rotation of the entire guidewire around its own axis. Thus, the hook formed by the guidewire changes direction and points in the opposite one, as illustrated in Fig. 2. This technique, relying on a S-shaped active double curve at the distal tip, appears to be an efficient maneuver to stabilize the device within the aortic arch and point into a selected SAT ostium.

### 2.3. Gestures by the clinician

As explained, in the case of navigation with active devices towards complex targets, clinicians perform many movements including rotations in addition to distal tip actuation. To correctly simulate

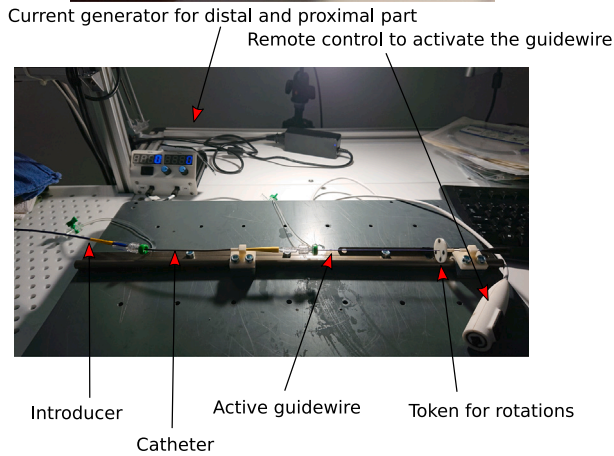


Fig. 3. Additional set-up to measure clinician movements during navigation: instrumentation of the BCV bench.

the insertion of surgical tools, we aimed at determining an order of magnitude of the velocities applied to the devices.

These velocities were established thanks to a set-up added to the existing test bench presented in Fig. 3.

It consisted of two bearings sliding on a 500 mm rail. One of them was attached to the catheter, and the other to the proximal part of the guidewire. Targets were stuck to the bearings and a camera was able to track the movements on both the catheter and the guidewire. For the rotation of the guidewire, a stained token was attached to the shaft with adhesive tap. An other camera tracked the rotations. The frequency of the two cameras was 10 Hz. Two additional cameras recorded the navigation through the aorta. As the activation of the guidewire consisted of applying a current, a last camera focused on an LCD screen displaying the electric current injected in the proximal and the distal moduli as well as the hands of the clinicians.

Several navigations with the goal of reaching the left carotid artery were filmed. Sequences were sorted and we computed an average velocity for the various phases as presented in Table 1. All the measurements were performed on the same phantom (named PY aorta for the anatomy of the patient PY, see Fig. 7).

### 3. Methods

Once the main features of navigation as performed by surgeons were characterized, we built a numerical model based on the Finite

Table 1

Mean velocities of the clinician gestures during active navigation.

| Movement           | Speed values<br>(mm/s and °/s) | Description<br>(see Fig. 5) |
|--------------------|--------------------------------|-----------------------------|
| Pushing guidewire  | $21.4 \pm 5.1$                 | PushG                       |
| Pushing catheter   | $-13.5 \pm 4.2$                | PushC                       |
| Pulling guidewire  | $12.3 \pm 4.6$                 | PullG                       |
| Rotating guidewire | $210.9 \pm 80.4$               | RotG                        |

Element Method (FEM) to simulate this navigation and validate it against observations on the test bench.

#### 3.1. Tools modeling

**Geometry.** The model includes the active guidewire, a Navien catheter and a Neuron introducer. Fig. 4 describes their dimensions.

The lengths  $d$ ,  $L_p$ ,  $L_d$  and the distance  $e$  between the two active parts could be changed in the guidewire design. The total length of the distal part was 73 mm. The distal tip of the guidewire included active parts where the Nitinol wires were connected to the blade by rigid links. The gap between the blade and the Nitinol wires was set to 0.285 mm. The stiffness of the blade varied depending on the area. The three different areas are highlighted in Fig. 4. When the Nitinol wires are present on both sides of the blade (in the so-called overlap area), the area is considered stiffer than the other parts and inactive. The mechanical properties of the different portions of the blade were determined in Badrou et al. (2022). The overlap area was characterized using 3-point bending tests. The catheters are made of several portions of varying stiffnesses that have been characterized in a previous study through 3-point bending tests (Badrou et al., 2022). All the mechanical properties of the tools are summarized in Table 2.

The full length of the different tools was not modeled. Indeed, due to a narrow entrance of the descending aorta visible in Fig. 1, we assumed in the case of simulating the experimental navigation, that the length outside the box had no effect on the navigation itself. A sufficient length was adjusted to allow the navigation to the left carotid.

**Mesh.** The FEM was chosen to simulate the navigation. We used Hughes–Liu beam elements in Ls-Dyna (Ansys/LST, CA., USA, 1976) for the guidewire. The wire and the blade (distal tip) were meshed with a 1-mm beam. Beam elements of 2 mm were chosen for the shaft. The mesh size for the tools and the aorta was determined based on a convergence analysis on aorta PY, see Supplementary Material. One integration point was used for the Nitinol wires in order for them to act as bar elements and the overall rigidity of active parts was borne by the blade in green.

The catheters and the introducer were meshed with fully integrated shell elements to avoid Hourglass modes. Belytschko–Tsay shells which are of the type Reissner–Mindlin were preferred for the introducer. The number of integration points was fixed to three which was clearly enough for the thickness of the elements.

**Material law.** Because of the complex composition of the catheters, some parts (mainly the distal one) exhibited a viscoelastic behavior modeled by a generalized Maxwell formula with one element (Herrmann and Peterson, 1968):

$$G(t) = G_\infty + (G_0 - G_\infty)e^{-\beta t}$$

Here,  $G_\infty$  and  $G_0$  were respectively the long and short time shear modulus, and the parameter  $\beta$  was a constant expressed per unit of time.

The other parts were assumed to be elastic. Table 2 lists the material parameters for the Navien catheter, the introducer and the guidewire components depending on their elastic or viscoelastic behavior.

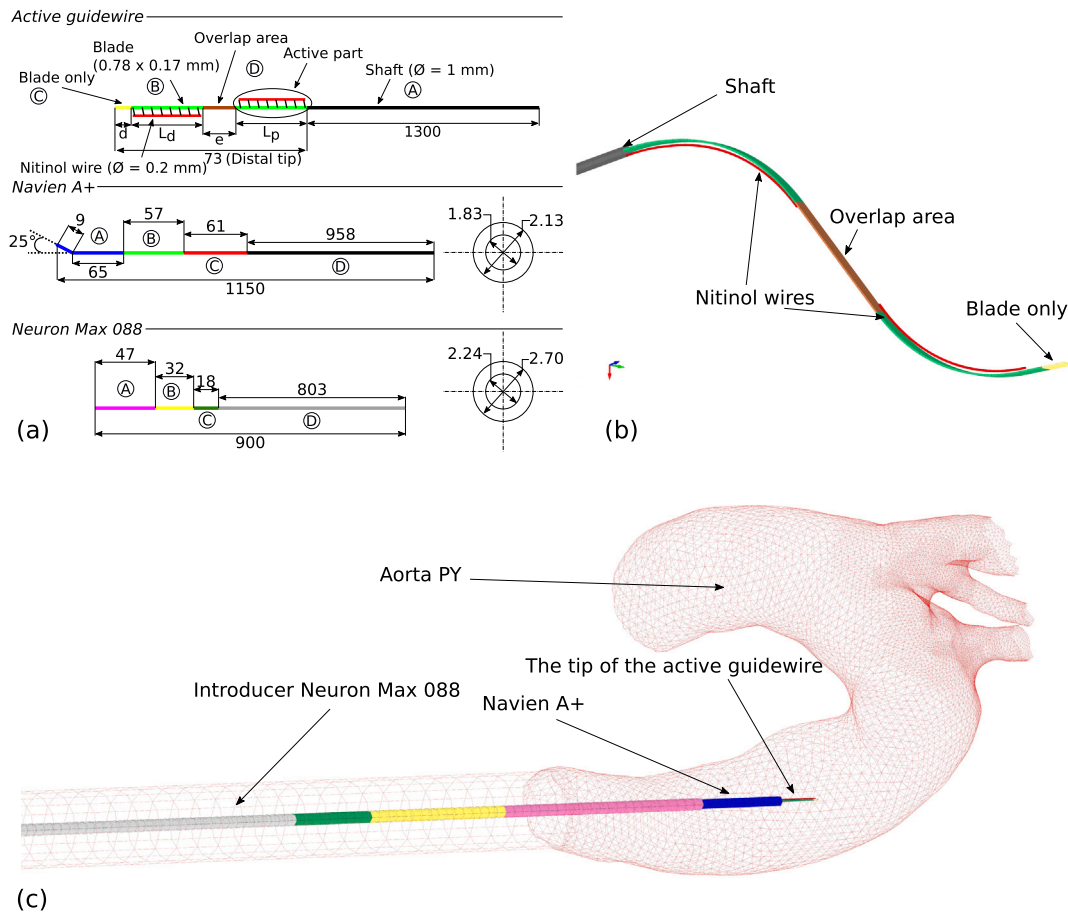


**Fig. 4.** (a) Devices dimensions of the model: active guidewire and catheters used in our case. For each tool, the colors describe various portions having their different mechanical properties. Each portion is identified by a letter (from A to D) which refers to Table 2 presenting the properties of the devices. (b) Visualization of the guidewire distal tip when activated: when the Nitinol wires are heated, they shrink making the blade (green parts) bend. (c) Assembly of the different tools (introducer + catheter + guidewire) in the PY aorta for the endovascular navigation.

**Table 2**  
Mechanical properties along the surgical tools: Areas A to D are related to those in Fig. 4.

|                  | A   | B   | C   | D   |
|------------------|---|---|---|---|
| Active guidewire | $E = 8047.8 \text{ MPa}$<br>$\nu = 0.3$   | $E = 71130.0 \text{ MPa}$<br>$\nu = 0.3$  | $E = 52720.0 \text{ MPa}$<br>$\nu = 0.3$  | $E = 175000.0 \text{ MPa}$<br>$\nu = 0.3$ |
| Navien           | $\beta = 0.22 \text{ s}^{-1}$<br>$G_0 = 62.0 \text{ MPa}$<br>$G_\infty = 15.9 \text{ MPa}$<br>$B = 82.9 \text{ MPa}$  | $\beta = 0.16 \text{ s}^{-1}$<br>$G_0 = 94.1 \text{ MPa}$<br>$G_\infty = 26.6 \text{ MPa}$<br>$B = 152.3 \text{ MPa}$ | $\beta = 0.18 \text{ s}^{-1}$<br>$G_0 = 448.1 \text{ MPa}$<br>$G_\infty = 152.2 \text{ MPa}$<br>$B = 694.6 \text{ MPa}$ | $E = 1519 \text{ MPa}$                    |
| Neuron           | $\beta = 0.26 \text{ s}^{-1}$<br>$G_0 = 74.0 \text{ MPa}$<br>$G_\infty = 17.0 \text{ MPa}$<br>$B = 122.1 \text{ MPa}$ | $E = 250 \text{ MPa}$   | $E = 180 \text{ MPa}$   | $E = 1701 \text{ MPa}$                    |

As discussed previously, the guidewire was an active steerable device, and its curvature could be controlled thanks to the SME. To model this particular behavior, we implemented a 1D law described by Tanaka et al. (1986) in Ls-Dyna, following studies previously conducted by Ianucci et al. (2017). To represent the actuation of the Nitinol wires, we implemented a 1D law described by Tanaka et al. (1986) in Ls-Dyna, following studies previously conducted by Ianucci et al. (2017). The description of the law is given in Appendix. We used this law in a simplified way: we were interested in the guidewire curvature (corresponding to the maximum recoverable strain of the wire  $\epsilon_L$ ) as well as activation/deactivation times ( $t_a$  and  $t_d$  respectively). Therefore, we identified parameters  $\epsilon_L$ ,  $t_a$  and  $t_d$  using the experiments presented

in Badrou et al. (2022). Then, in the simulation, we imposed to the Nitinol wires a temperature load  $T$  as a linear function of time between  $37^\circ\text{C}$  and  $65^\circ\text{C}$ . The time intervals from one temperature to the other were defined to respect  $t_a$  and  $t_d$ . The wire model provided a longitudinal strain leading to the device bending, until reaching  $\epsilon_L$ . This way of using Tanaka's law is equivalent to drive the wire strain by displacement; however, we used Tanaka's law so that our model is easily adaptable to a full description of SME. From Badrou et al. (2022), we determined that  $\epsilon_L = 0.0347$  and  $t_a = t_d = 1.7\text{s}$  for the guidewire design tested in this paper. We indeed observed experimentally that, due to the blade elasticity which brings the wire back to its initial configuration at deactivation, the activation and deactivation times are

very similar.  $\epsilon_L$  is a design parameter that can be tuned to adapt to the considered patient as we will see in Section 4.2.

### 3.2. Aortic phantoms modeling

**Geometry.** Three phantoms were available for the test bench, based on patient cases (patients PY, LP and FM). The same geometries were used in the model. They were classified by surgeons in our group as “complex” because the insertion point in order to reach the left carotid was difficult to access (see Fig. 7). These are typically complex anatomical cases in which navigation with passive tools would most probably fail. Indeed, for the aorta PY, the anchor point for hooking the carotid artery is low compared to the dome of the aortic arch. The aorta FM has a bovine arch: the innominate artery shares its origin with the left carotid. The origin of the carotid in the aorta LP is narrow and is not aligned with the insertion points of neighboring arteries.

**Mesh.** The different geometries were meshed based on a mesh sensitivity analysis. We chose to use Belytschko–Tsay triangular shell elements. Since we were interested in hooking the left carotid we decided to finely mesh the areas near the SAT to catch the tortuosities. The chosen mesh size was 0.5 mm on these areas. A transition area with a mesh size of 1 mm was applied and the rest of the aorta was meshed with 2-mm elements for contact management. The thickness of the aortas varied from 2 to 4 mm on the BCV test bench. We decided to fix an average thickness for the overall aortas of 3 mm.

**Material law.** The aortas were assumed to be rigid.

### 3.3. Boundary conditions and numerical parameters

Fig. 5 depicts the boundary conditions at the entrance of the descending aorta model for the surgical tools.

Nodes of the catheter and introducer in area 5 were fixed in displacements in X and Y and in rotation around the X and Y axis. These particular conditions were due to the narrow entrance (see Fig. 1) that constrained the devices. The proximal end of the catheter (nodes of areas 3) was constrained in all directions when the guidewire was moving. Nodes of area 4 were fixed. Indeed these ends were assumed to be held by the handler. The end of the guidewire (area 1) was presumed to move only along the Z axis and rotate around it. A rotation speed was applied on nodes of area 2 and a linear velocity command on those of area 1, their amplitude is given in Table 1. Regarding the contact between the materials, frictional forces were assumed to be present both between the tools themselves and between the tools and the aorta. We used a penalty method to represent the contact and a friction coefficient of 0.2 was set by default except between the guidewire and the aorta and between the catheter and the introducer where the friction coefficient was set to 0.3 and 0.1, respectively. Mass scaling was employed with a given time step of  $5 \cdot 10^{-6}$ s. To stabilize the active guidewire during the navigation, Rayleigh damping was used by playing of the mass proportional damping coefficient. We see in Fig. 7 that damping energy as kinetic energy are low compared to internal energy which confirms the validity of the damping and mass scaling levels adopted for this study.

## 4. Results

### 4.1. Validation

In order to validate the simulation of the endovascular navigation through phantom aortas, we simulated the insertion of the surgical tools into the aorta PY with regard to the experimental navigation. The inputs followed the path-based gestures of the clinicians. Validation was conducted on passive sequences (back and forth movements were applied to the guidewire without any activation), and on active sequences in which the device was actively bent. Attention was paid to several actions and phenomena occurring in reality:

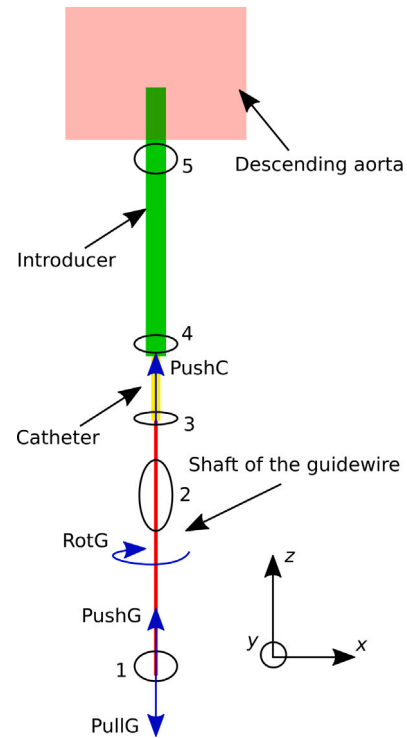


Fig. 5. Boundary conditions applied on the devices during endovascular navigation. PushC, PushG, PullG and RotG are related to Table 1 defining the different movements and their value.

- Passive navigation: by pushing, pulling or rotating the devices without any activation;
- Activation of the active parts: the distal tip of the guidewire curves in a multi-curve way;
- Snapping.

We tried to correctly represent these phenomena in simulation. Fig. 6 compares the guidewire position between simulation and real navigation on the test bench during both passive and active sequences. For active sequences, we also followed the tip of the guidewire and recorded its coordinates with the camera plane of the test bench. The results show good agreement between the two datasets, a slight position deviation can be seen on the guidewire just after snapping but it did not affect the final position.

The model parameterization made it possible to reproduce the various phenomena observed experimentally: snapping, active curvatures, interactions between the tools. Now that navigation within a phantom could be reduced, we wanted to make use of this simulation as a design assistance tool to find a combination of guidewire design parameters that would make it possible to hook the left carotid in different anatomies.

### 4.2. Application: simulation of endovascular navigation in two additional complex aortas

For the PY aorta, “clinical” gestures were measured and combinations of sequences could be reproduced. For the two other aortas, we relied on the previously validated simulator to find appropriate navigation parameters and guidewire design specifications to hook the left carotid.

The parameters on which we acted were the lengths  $L_p$ ,  $L_d$ ,  $e$  and the maximum recoverable strain  $\epsilon_L$ . The latter parameter concerned the ability of the Nitinol wire to contract exhibiting a change in the current intensity or in the grade of SMA. The values used to achieve hooking were determined by trial and error.

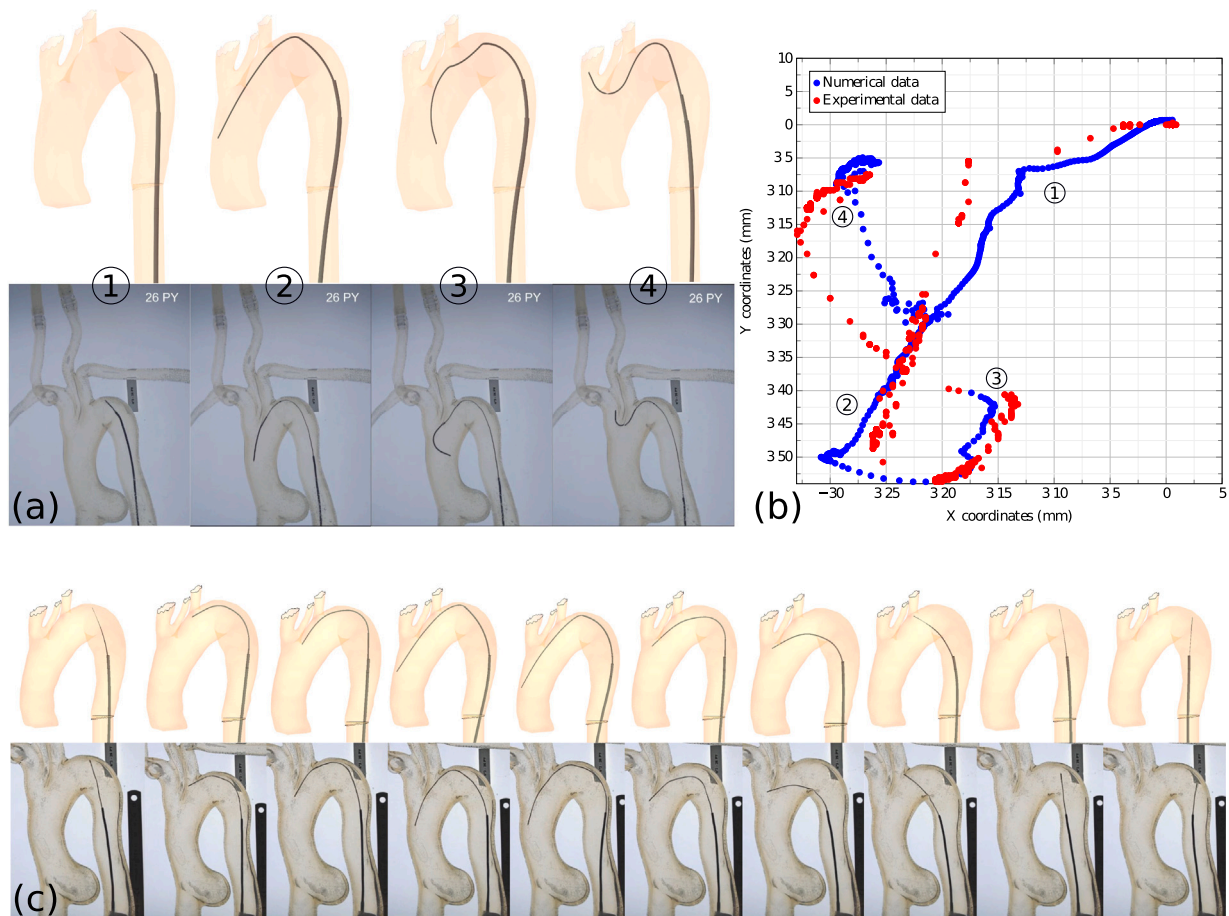


**Fig. 6.** (a) Validation of the active navigation into the phantom aorta PY at different stages. (b) Guidewire tip coordinates during endovascular navigation in the camera plane: comparison between numerical (top) and experimental (bottom) data. The guidewire navigation begins at the top of the aortic arch in ① until it contacts the descending aorta in phase ②. In step ③ the guidewire is activated and “snaps” to reach the SATs in ④. (c) Passive navigation is compared between numerical (top) and experimental (bottom) data in the PY aorta.

For the navigation into the PY and FM aorta, the boundary conditions were quite similar: the guidewire was pushed until the distal tip was in the ascending aorta, the parts were activated and the guidewire was snapped. The device was then pulled in order to hook the left carotid. Regarding the LP aorta, the active parts did not overlap (blade only) and the distance between them,  $e$ , was long. No snapping was used in this case. The proximal modulus helped to curve the distal part of the guidewire and the distal modulus made it possible to point to the entrance of the carotid.

Fig. 7 shows that we were able to hook the left carotid for all cases despite their complexity, demonstrating the potential of the simulation to provide guidance into navigation gestures and device design.

## 5. Discussion

### 5.1. Main results

This article describes the development of a numerical model of endovascular navigation involving an active guidewire and catheters to cerebral targets. To the best of our knowledge, this is the first simulation combining an active steerable device, a catheter and their interactions with the vascular environment. In order to create the model, a complete characterization of the navigation was conducted. This work enabled (i) a better overview of the effects occurring during active navigation, such as snapping, and (ii) measurements of the velocities imposed by the clinicians to the surgical tools thanks to an original set-up.

Indeed, during endovascular navigation many movements are imposed on the tools. It is thus crucial to have an order of magnitude of the velocities for pulling, pushing and rotating the tools as well as for the sequences. Thus, an additional set-up was added to the phantom aorta test bench and several navigations from experienced handlers were recorded. In particular, experimental analysis was carried out of the snapping phenomenon. Through observation and simulation we investigated the reasons of this buckling in rotation and we found that snapping occurs when the proximal active modulus is directly connected to the shaft and activated after the guidewire contacts the aorta distally.

Regarding the experimental point of view, we performed a 3-point bending test on a portion of the phantom aorta and found a Young modulus of 4.3 MPa. The idea was to confirm the hypothesis of a rigid aorta in our model. Therefore, we compared the final position of the guidewire's distal part when navigating into the PY aorta between a rigid vs deformable aorta (phantom). The difference in position was computed using the Modified Hausdorff Distance (MHD) (Dubuisson and Jain, 1994). A value of MHD less than 1 mm was obtained and the assumption of a rigid aorta was therefore considered acceptable. Of course, this assumption can be questioned when it comes to real patient data and a probably less stiff aortic wall, but this present work only focused on simulating a phantom aorta test bench.

We could thus create the endovascular navigation model based on this result and the experimental characterization. The model was validated with regard to the experimental navigation into a complex

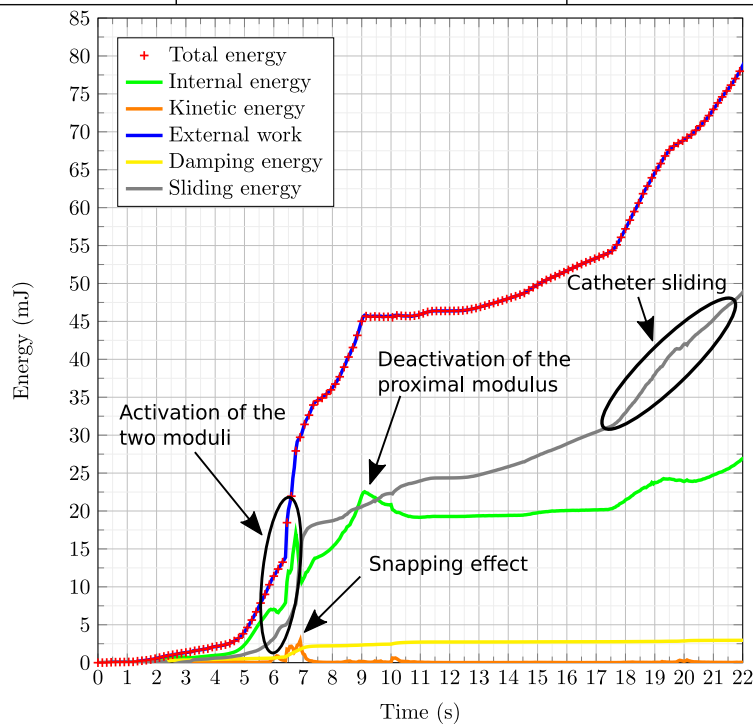
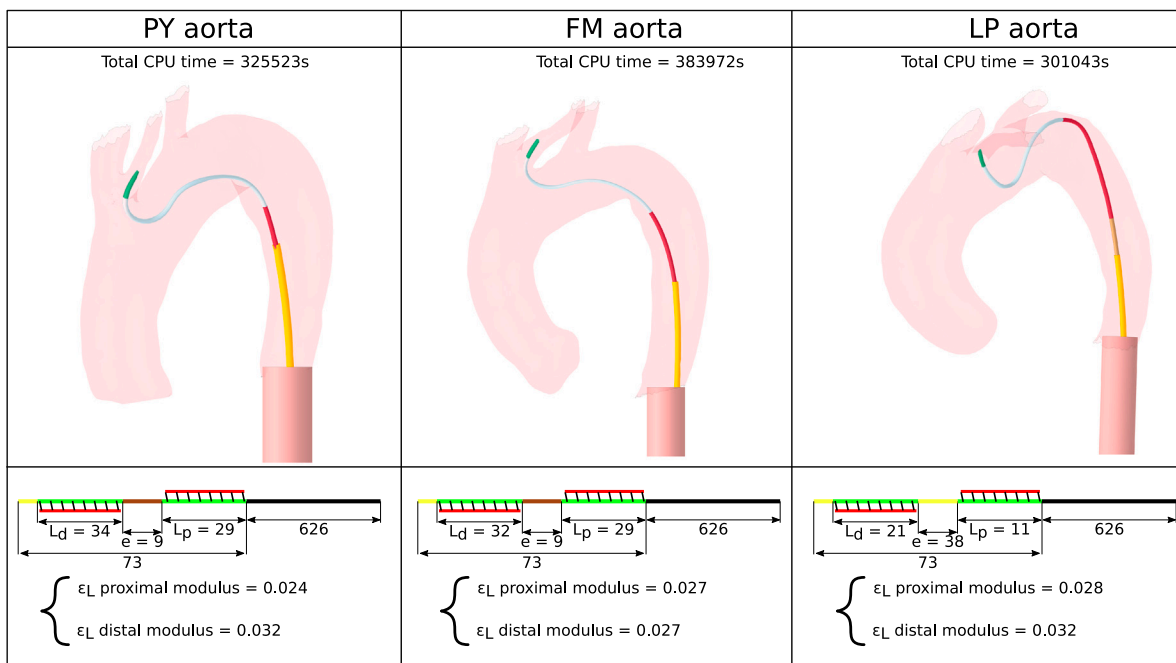


Fig. 7. Hooking of three complex aortas with details of the guidewire configuration used in each case.  $\epsilon_L$  is the maximal recoverable strain. CPU times using six Xeon 2.30 GHz cores are indicated. Graph of energies are plotted for the navigation into the PY aorta: the active guidewire first crosses the aortic arch until it is located nearby the left carotid artery. The two moduli are activated and the snapping effect occurs (kinetic energy peak). The active guidewire is pulled and the proximal modulus is deactivated. The left carotid is hooked and the Navien catheter slides on the guidewire to reach the carotid. The navigation sequences were similar for the other aortas.

aorta and particular attention was paid to the representation of experimentally observed phenomena such as the activation of the guidewire, passive navigation or the snapping effect.

Once our model was set-up, we demonstrated that hooking the left carotid was partially driven by the guidewire design. Among the various parameters, we acted on five parameters specific to the guidewire. Thanks to different configurations we succeeded in hooking three highly complex anatomies. Among these design parameters,  $\epsilon_L$  is probably the most challenging as it reflects both material (Nitinol grade) and activation (current intensity) features. It is also affected by fatigue.

Hence, preliminary tests would probably be necessary to reach the targeted value of  $\epsilon_L$  during design.

### 5.2. Study limits

The blood flow in the aortic arch is pulsed and considered to be turbulent (Menut, 2017). This particular flow may have an impact on navigation. The flow applied to the test bench was low compared to real conditions and in simulation and the bloodstream was not taken into consideration at all in the simulation. Moreover, navigation tests on animals were conducted by the team and it was observed that blood

flow and aortic wall deformations could probably be neglected because of their small influence on the guidewire position.

Concerning the geometries of the surgical tools involved in the simulation, we did not represent the total lengths of the devices. We can consider that it did not have any consequences related to the gestures of the clinician: during experimental navigation, handlers navigate near the hemostatis valve to reduce the risk of buckling when it comes to linear movements. But the rotations are applied close to the proximal end of the shaft whereas in our model they are applied near the valve. This difference resulted in a shorter turnaround time in simulation but did not affect the navigation itself. Regarding the experimental results on the measurement of the clinician gestures, the uncertainties were large due to a low amount of data and to movements that were difficult to repeat (especially the rotations). However, the success of navigation was not limited to a few speed values but rather allowed for a wide range of speeds. For our simulations, we considered average velocities.

The simulation was performed on the same patient-specific geometries as the ones used to create the phantoms for validation purposes. However, the geometries slightly differ. Indeed, the Supra-Aortic Trunks (SATs) and the ascending aorta are shorter in the numerical model. Manufacturing phantoms also generates small inaccuracies, that can be visible at the junction between the SATs and the aortic arc and in the descending aorta for instance. However, we consider that the experimental and simulation geometries are close enough to ensure a satisfactory validation of the navigation related to this study.

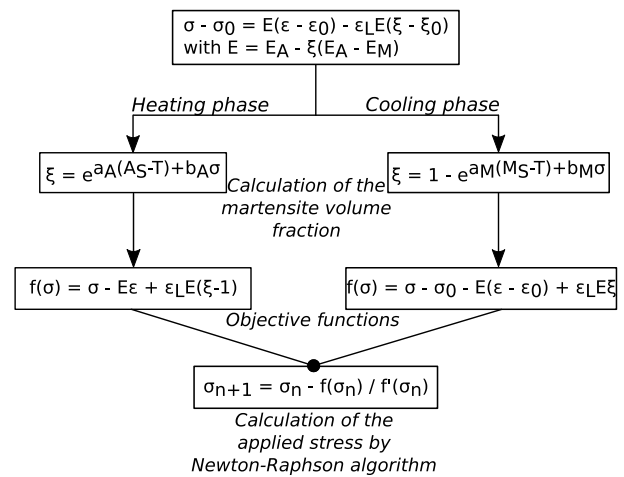
A rigid aorta clearly differs from real aorta modeling (Labrosse et al., 2009). The simulations were therefore not transferable to a clinical situation. But in reality, the aortic arch is quite rigid, thus, the position of the guidewire should not be too far from the one obtained with a simulation on a rigid aorta. Nevertheless, this requires further validation against patient data.

Validation was performed in different configuration based on displacements only. It showed that the passive behavior of the guidewire is mechanically reasonable as the guidewire deformation due to contact with the aortic walls is accurately simulated. However, concerning activation as previously discussed, the constitutive law used to represent the wire behavior is equivalent to a displacement-driven one. Therefore, in the simulation, the curved guidewire would impose its motion to its environment and generate very high reaction forces; this is obviously not realistic and unfit for validation. We anyway used this model as it was shown both on phantom experiments and animal experiments that the activated guidewire is indeed very stiff compared to the surrounding tissue and tools.

## 6. Conclusion

This paper presents a numerical model of active endovascular tools navigating towards complex targets. It is based on patient specific anatomies and experimental characterization of both the tools and the praticians's gestures. Now that is has been shown that complex anatomies can be successfully navigated on the test bench and in simulation, two main perspectives can be drawn:

1. For design purposes and surgeons training, the numerical model could be generalized to a larger cohort of anatomy using for example learning or reduced order modeling approaches (Lu et al., 2017a,b);
2. For clinical application purposes, the model could be adapted to real patient cases provided some assumptions regarding for example material models, boundary conditions or effect of blood flow are further questioned.



| Parameter               | Description                                 | Value                              |
|-------------------------|---|------------------------------------|
| $E_A$                   | Austenite Young modulus                     | 50000 MPa                          |
| $E_M$                   | Martensite Young modulus                    | 33320 MPa                          |
| $\epsilon_L$            | Maximum recoverable strain                  | 0.0347                             |
| $M_{s/f}$               | Martensite starting / finishing temperature | 47 / 43 °C                         |
| $A_{s/f}$               | Austenite starting / finishing temperature  | 60 / 65 °C                         |
| $T_{(de)activation}$    | Time required to bend the guidewire         | 1.7 s                              |
| $a_A ; a_M ; b_A ; b_M$ | Material constants                          | 0.92 ; -1.15 ; 0.11 ; -0.14 (1/°C) |

Fig. A.8. Overview diagram of Tanaka's law and parameters used in our case. In the diagram, the parameters  $(-)_0$  are related to the initial conditions. The applied stress  $\sigma$  was determined by Hooke's law added to a temperature dependent term. Depending on whether the material was heated or cooled, the martensite volume fraction  $\xi$  was computed using the temperature  $T$  and material constants  $a_A, a_M, b_A, b_M$  which are function of the starting/ending temperatures of the different phases. Finally, objective functions were created and a Newton-Raphson algorithm was used to compute the stress at the next time step.

## CRediT authorship contribution statement

**Arif Badrou:** Writing – original draft, Methodology, Data curation. **Nicolas Tardif:** Writing – review & editing, Supervision, Methodology. **Philippe Chaudet:** Methodology. **Nathan Lescanne:** Methodology. **Jérôme Szewczyk:** Writing – review & editing, Supervision. **Raphaël Blanc:** Methodology. **Nahiène Hamila:** Writing – review & editing, Methodology. **Anthony Gravouil:** Writing – review & editing, Methodology. **Aline Bel-Brunon:** Writing – review & editing, Writing – original draft, Supervision, Methodology.

## Declaration of competing interest

The authors declare that they have no known competing financial interests or personal relationships that could have appeared to influence the work reported in this paper.

## Acknowledgments

The French National Research Agency (ANR), France partially supported this work through the DEEP project: Devices for augmEnted Endovascular navigation in complex Pathways (grant n° ANR-18-CE19-0027-01).

See Fig. A.8.

## Appendix B. Supplementary data

Supplementary material related to this article can be found online at <https://doi.org/10.1016/j.jbiomech.2022.111147>.

## References

- Alderliesten, T., Konings, M.K., Niessen, W.J., 2004. Simulation of minimally invasive vascular interventions for training purposes. *Comput. Aided Surg.* 9, 3–15.
- Ali, A., Szili-Torok, T., Stijnen, M., Breedveld, P., Dodou, D., 2020. First expert evaluation of a new steerable catheter in an isolated beating heart. *Cardiovasc. Eng. Technol.* 11, 769–782.
- Auricchio, F., Conti, M., Marconi, S., Reali, A., Tolenaar, J.L., Trimarchi, S., 2013. Patient-specific aortic endografting simulation: From diagnosis to prediction. *Comput. Biol. Med.* 43, 386–394.
- Badrou, A., Tardif, N., Even, A., Chaudet, P., Lescanne, N., Szewczyk, J., Gravouil, A., Hamila, N., Bel-Brunon, A., 2022. Characterization of Surgical Tools for Specific Endovascular Navigation. *Cardiovascular Engineering and Technology*.
- Couture, T., Szewczyk, J., 2017. Design and experimental validation of an active catheter for endovascular navigation. *J. Med. Dev.* 12.
- Dubuisson, M.P., Jain, A., 1994. A modified Hausdorff distance for object matching. In: *Proceedings of 12th International Conference on Pattern Recognition*, vol. 1, pp. 566–568.
- Ganet, F., Le, M.Q., Capsal, J.F., Lermusiaux, P., Petit, L., Millon, A., Cottinet, P.J., 2015. Development of a smart guide wire using an electrostrictive polymer: option for steerable orientation and force feedback. *Sci. Rep.* 5 (18593).
- Gindre, J., Bel-Brunon, A., Rochette, M., Lucas, A., Kaladji, A., Haigron, P., Combescure, A., 2016. Patient-specific finite-element simulation of the insertion of guidewire during an EVAR procedure: Guidewire position prediction validation on 28 cases. *IEEE Trans. Biomed. Eng.* 64, 1057–1066.
- Haga, Y., Tanahashi, Y., Esashi, M., 1998. Small diameter active catheter using shape memory alloy. In: *Proceedings MEMS 98. IEEE. Eleventh Annual International Workshop on Micro Electro Mechanical Systems. an Investigation of Micro Structures, Sensors, Actuators, Machines and Systems (Cat. No.98CH36176)*. pp. 419–424.
- Hashimoto, J., Ito, S., 2010. Pulse pressure amplification, arterial stiffness, and peripheral wave reflection determine pulsatile flow waveform of the femoral artery. *Hypertension* 56, 926–933.
- Herrmann, L.R., Peterson, F.E., 1968. *A Numerical Procedure for Viscoelastic Stress Analysis*, Orlando, FL.
- Hwang, J., Kim, Choi, H., 2020. A review of magnetic actuation systems and magnetically actuated guidewire- and catheter-based microrobots for vascular interventions. *Intell. Serv. Robot.* 13, 1–14.
- Ianucci, L., Robinson, P., Wan, A., Hamid, W., 2017. The Development of a User Defined Material Model for NiTi SMA Wires.
- Kaladji, A., Duménil, M., Castro, A., Cardon, A., Becquemin, J.P., Bou-Saïd, B., Lucas, A., Haigron, P., 2013. Prediction of deformations during endovascular aortic aneurysm repair using finite element simulation. *Comput. Med. Imaging Graph. : Offic. J. Comput. Med. Imaging Soc.* 37.
- Labrosse, M., Beller, C., Mesana, T., Veinot, J., 2009. Mechanical behavior of human aortas: Experiments, material constants and 3-D finite element modeling including residual stress. *J. Biomech.* 42, 996–1004.
- Lagoudas, D.C., 2008. *Shape Memory Alloys*, vol. 1. Springer US, Boston, MA.
- Lam, R.C., Lin, S.C., DeRubertis, B., Hyneczek, R., Kent, K.C., Faries, P.L., 2007. The impact of increasing age on anatomic factors affecting carotid angioplasty and stenting. *J. Vasc. Surg.* 45, 875–880.
- Lu, Y., Blal, N., Gravouil, A., 2017a. Construction d'abaques numériques pour des calculs en temps-réel : application au procédé de soudage.
- Lu, Y., Blal, N., Gravouil, A., 2017b. Multi-parametric space-time computational vademecum for parametric studies: Application to real time welding simulations. *Finite Elem. Anal. Des.* 139.
- Macdonald, S., Lee, R., Williams, R., Stansby, G., 2009. Towards safer carotid artery stenting. *Stroke* 40, 1698–1703.
- Madhwal, S., Rajagopal, V., Bhatt, D., Bajzer, C., Whitlow, P., Kapadia, S., 2008. Predictors of difficult carotid stenting as determined by aortic arch angiography. *J. Invasive Cardiol.* 20, 200–204.
- Maynadier, A., Depriester, D., Lavernhe-Taillard, K., Hubert, O., 2011. Thermo-mechanical description of phase transformation in Ni-Ti Shape Memory Alloy. *Procedia Eng.* 10, 2208–2213.
- Menut, M., 2017. *Chirurgie Endovasculaire Virtuelle Pour Patient-Spécifique : Application Au Traitement de L'anévrisme de L'Aorte Thoracique (Ph.D. thesis)*.
- Mohammadi, H., Lessard, S., Therasse, E., Mongrain, R., Soulez, G., 2018. A numerical preoperative planning model to predict arterial deformations in endovascular aortic aneurysm repair. *Ann. Biomed. Eng.* 46, 2148–2161.
- Mouktadiri, G., Bou-Saïd, B., Walter-Le-Berre, H., 2013. Aortic endovascular repair modeling using the finite element method. *J. Biomed. Sci. Eng.* 06, 917–927.
- Nesbitt, C., Birdi, N., Mafeld, S., Stansby, G., 2016. The role of simulation in the development of endovascular surgical skills. *Perspect. Med. Educ.* 5.
- Perrin, D., Badel, P., Avril, S., Albertini, J.N., Orgéas, C., Duménil, C., 2014. Patient-specific simulation of stent-graft deployment within an abdominal aortic aneurysm.
- Roy, D., Holzapfel, G.A., Kauffmann, C., Soulez, G., 2014. Finite element analysis of abdominal aortic aneurysms: geometrical and structural reconstruction with application of an anisotropic material model. *IMA J. Appl. Math.* 79, 1011–1026.
- See, K., Chui, K., Chan, W., Wong, K., Chan, Y., 2016. Evidence for endovascular simulation training: A systematic review. *Eur. J. Vasc. Endovasc. Surg.* 51, 441–451.
- Sochi, T., 2013. Non-Newtonian rheology in blood circulation.
- Spiotta, A.M., Hussain, M.S., Sivapatham, T., Bain, M., Gupta, R., Moskowitz, S.I., Hui, F.K., 2011. The versatile distal access catheter: The Cleveland clinic experience. *Neurosurgery* 68, 1677–1686.
- Szewczyk, J., 2011. *Process for Manufacturing a Flexible Elongate Structure Having an Orientable End*.
- Szewczyk, J., Marchandise, E., Flaud, P., Royon, L., Blanc, R., 2011. Active catheters for neuroradiology. *J. Robot. Mechatron.* 23, 105–115.
- Tanaka, K., Kobayashi, S., Sato, Y., 1986. Thermomechanics of transformation pseudoelasticity and shape memory effect in alloys. *Int. J. Plast.* 2, 59–72.
- Verhage, R., Hazebroek, E., Boone, J., van Hillegersberg, R., 2009. Minimally invasive surgery compared to open procedures in esophagectomy for cancer: A systematic review of the literature. *Minerva Chirurgica* 64, 135–146.
- Vy, P., Auffret, V., Castro, M., Badel, P., Rochette, M., Haigron, P., Avril, S., 2018. Patient-specific simulation of guidewire deformation during transcatheter aortic valve implantation. *Int. J. Numer. Methods Biomed. Eng.* 34, e2974.
- Wayman, C.M., Duerig, T.W., 1990. An introduction to martensite and shape memory. In: *Duerig, T.W., Melton, K.N., Stöckel, D., Wayman, C.M. (Eds.), Engineering Aspects of Shape Memory Alloys*. Butterworth-Heinemann, pp. 3–20.
- Westwood, J., 2005. *Medicine Meets Virtual Reality 13: The Magical Next Becomes the Medical now. Medicine Meets Virtual Reality*. 13, IOS.